Thermochemical modeling and performance evaluation of freeze desalination systems

Aly Elhefny, Hamidreza Shabgard*, Jie Cai, Reza Kaviani, Ramkumar N. Parthasarathy

University of Oklahoma, Norman, OK, 73019, USA

Abstract

Freeze desalination (FD) is a method in which saline water is cooled below its freezing point and freshwater is separated from the brine in the form of ice crystals. FD is relatively insensitive to the salinity of the feed solution, making it suitable for desalination of high concentration brines such as the brine rejected from the seawater desalination plants. The design of the FD system and the thermochemical behavior of the brine upon freezing are critical factors in the energy performance of this method. To date, thermochemical properties of the concentrated seawater during cooling, such as the threshold of formation of ice and salt-hydrates and their corresponding cooling load of formation, are not well known. Likewise, the optimal configuration of the FD system to achieve the maximum energy efficiency has not been investigated. This work provides comprehensive data about the cooling load of freezing of concentrated brine rejected from seawater desalination plants along with the threshold of formation of ice and salt-hydrates backed-up by validation. Furthermore, the optimal configuration of the FD system is identified and the effects of the compressor isentropic efficiency and effectiveness of the system's heat exchangers on the work consumption of the FD system were investigated.

KEYWORDS: Freeze desalination; Co-simulation; Energy efficiency; Brine thermo-chemical properties; Brine cooling load; System configuration

Nomenclature

C	specific heat [J/kg°C]
G	excess Gibbs free energy [J/mol]
h	enthalpy [J/kg]
h_{sl}	latent heat of fusion [J/kg]
m	mass flow rate [kg/s]
Q	heat transfer rate [W]
R	water recovery ratio
R_g	gas constant [J/mol-K]
S	salinity [ppm]
T	temperature [°C]
T_K	temperature [K]
T_m	melting temperature at brine concentration value [°C]
UA	overall heat transfer coefficient [W/°C]
u	fluid velocity in the x direction [m/s]
W	work [W]

Greek symbols

$\eta_{isentropic}$	isentropic efficiency [%]
γ	activity coefficient
ϕ_{ice}	ice (solid pure H_2O) mass fraction

1

Subscripts

a	ambient
c	condensing/ condenser
ch	brine freezing chamber
$comp$	compressor
e	evaporating/ evaporator
f	feed
fz	at the onset of freezing
H	at the high pressure side
i	inlet
L	at the low pressure side/ linked to the long-range ionic interaction
l	liquid phase
M	linked to the middle range ionic interactions
m	melting
o	outlet
min	Minimum
r	refrigerant
rb	rejected brine
S	linked to the short-range ionic interactions
s	solid phase
st	fluid stream
tw	treated water
w	wall

2

Abbreviations

COP	coefficient of performance
FD	freeze desalination
ICL	intermediate cooling liquid
ppm	parts per million (unit)
$SFDW$	specific freeze desalination work consumption

1 Introduction

Fresh water shortage is a serious and fast-escalating global problem [1]. The population living in agricultural regions categorized by high to very high levels of water shortage is estimated at 1.42 billion [2]. By the year 2050, the number of people living in potentially water-scarce areas at least one month of the year is estimated to be 4.8-5.7 billion [3]. Desalination of seawater and impaired water from other sources is posed to play a critical role in meeting the increasing water demand [4].

Currently, reverse osmosis and thermal distillation are the dominant desalination technologies [5]. However, commercial membrane desalination technologies are limited to handling maximum water salinities around 70,000 ppm [6,7] and their performance dramatically degrades at higher brine concentrations [7-10]. The applicability of thermal desalination plants at higher salinities is constrained by extensive fouling and corrosion and relatively high energy consumption [11]. Freeze desalination (FD) is considered one of the emerging desalination technologies that can effectively address the above challenges [12-14]. The latent heat of solidification is relatively low compared to the heat of vaporization of seawater (the latent heat of solidification is about 1/7 of the latent heat of evaporation [15]). In addition, due to the low operating temperature and the absence of membranes, fouling and corrosion-related problems are minimal. There are two major categories for FD: direct FD, and indirect FD. In the case of direct FD, the refrigerant is in direct contact with the feed while in the case of indirect FD, there is a solid surface separating the refrigerant and the brine. Both direct and indirect FD are evolving technologies and have not reached industrial-scale application [16, 17] due to a few major issues and knowledge gaps [18].

One of the primary issues common for both direct and indirect FD is the difficulty in separation of the brine and salt-hydrates from the ice (pure H_2O in solid state). Another major issue linked to the direct FD is the presence of excessive amounts of undesirable refrigerant in the desalinated water, drastically degrading the quality of the treated water and adding more separation complexities [19]. On the other hand, since the indirect FD involves a solid surface separating the refrigerant and the brine during crystallization, the desalinated water is refrigerant-free [20]. The key disadvantage of indirect FD is that it is thermally less efficient than direct FD since ice formation on cooling surfaces deteriorates heat transfer and requires complex design to scrape the ice off the cold surfaces. To date, the energy performance of FD is not well understood due to limited knowledge of the behavior of brine upon freezing and the optimal configuration of the system [18]. This includes lack of knowledge about the brine's cooling load of freezing and thermo-chemical properties at different freezing temperatures of the system. This study contributes to a better understanding of the FD process by addressing the following primary knowledge gaps:

1. Knowledge about the concentrated seawater cooling load of freezing and threshold of freezing, where cooling the seawater results in variation of the cooling load of freezing and each of the salt-hydrates forms at a specific temperature, introducing a new source of thermal load that needs to be determined carefully for accurate energy analysis of FD systems. In addition, the study introduces knowledge about the concentrated seawater's other thermochemical properties.
2. Knowledge about the FD system's optimal configuration (most energy efficient configuration) and its optimal operational parameters along with the corresponding energy consumption performance.

The following sections of this study focus on addressing the FD system's research gaps described. In Section 2, the research problem is framed by discussing relevant issues and the adopted research approaches. In Section 3, the thermochemical behavior of seawater upon freezing is discussed. Section 4 highlights the optimal configuration of the FD system. Section 5 focuses on the thermochemical modeling of the FD system. Section 6 presents the results related to the work consumption performance of the FD system as well as the brine's cooling load of freezing along with the corresponding compound formation.

2 Contextualizing the Issues and Research Objectives

This section sets the stage for the findings of this paper through establishing the context and scope of the issues, highlighting the solutions novelty, and providing insight into the selected research methodology. As described in the previous section, the FD technology can effectively address the challenges linked to the currently adopted commercial desalination techniques [12-14]. However, utilizing the FD technology at an industrial scale is still unattainable due to major issues and knowledge gaps. The most prominent issue with the FD technology is the raised energy requirement (it consumes less energy than the evaporative techniques, yet the energy consumption is still high and the FD system's energy efficiency has not been previously optimized). The question is, what is the FD system's configuration that maximizes its energy efficiency ?. In FD technology, a dominant fraction of the consumed energy is used to achieve the low temperatures inside the freezing chamber. Therefore, to significantly enhance the energy efficiency of FD, the recovery of the cooling energy is indispensable. Vapor compression is a widely utilized energy efficient cooling technology that is suitable to provide cooling for FD. For an FD system cooled by vapor compression technology, cooling energy recovery can be realized in the condenser or through precooling the inlet brine feed. This builds an impression that an FD system configuration utilizing vapor compression technology with cooling energy recovery feature will raise the FD process' energy efficiency. Yet the FD system's configuration issue raised earlier cannot be fully addressed without answering the following questions:

- To maximize the FD system's energy efficiency, what is the best vapor compression system configuration to utilize (single stage/ cascade) ?
- What is the best approach for cooling energy recovery within the FD system to maximize its energy efficiency (cooling energy recovered in the condenser of the vapor compression cycle/ cooling energy recovered through precooling of the input brine) ?

This also raises a pivotal concern about selecting the optimal configuration of the FD system (the configuration with maximized energy efficiency). Given the large number of possible configurations for an FD system and the wide variety of components that can be utilized, how would we prove that a selected FD system configuration is the optimal one (such that -theoretically- no other FD configuration can prove more energy efficient) ?. To address that, we've decided to adopt theoretical analysis considering no irreversibility. The optimal FD system configuration can be identified when the theoretical outcomes converge with the published benchmark theoretical minimum work of separation for desalination (work required to ideally separate pure water from brine considering zero irreversibility) [21]. Different FD system configurations have been tested and the optimal configuration has been identified. The selection process is described through Appendix A and the FD configuration selected is meticulously described in Section 3. In addition, validation is presented in Section 6.2 to support the optimal FD system configuration claimed.

The optimal FD system configuration selected is generalized for direct and indirect FD systems. Yet if we adopt either of the two categories, we still need to address the relevant issues described in Section 1. For that, an innovative solution is adopted utilizing an intermediate cooling liquid (ICL) to overcome the described issues. The ICL is described in detail through Section 5.

Another issue is linked to the significant difficulty of separating the brine and salt-hydrates from the ice. Typically, a fraction of unfrozen brine gets carried over with the generated ice (will be described in detail through Section 4). The questions central to understanding the relevant knowledge gap encompass:

- What is the amount of the unfrozen brine carried over with the formed ice ?
- What are the FD system parameters affecting the amount of unfrozen brine carried over with the formed ice ?
- How would the unfrozen brine carried over with the generated ice affect the treated water salinity collected at the output of the FD system ?

In answer to these questions, Section 4 presents detailed analysis supported by the proofs of Appendix B.

As described in Section 1, two crucial knowledge deficiencies associated with FD when utilized to treat seawater brine, are the knowledge about the concentrated seawater cooling load of freezing and the concentrated seawater's thermochemical properties. Although some studies reported limited data about each of those two points, the published work does not include comprehensive data along the temperature range between 0ºC and -35ºC. This is extensively addressed throughout Section 6 based on the developed and validated model presented in Section 5. Furthermore, the work associated with the optimal FD configuration identified in this study has never been reported previously. Section 6 reports the work associated with the optimal FD system configuration considering the two primary sources of irreversibility and brine feed with different concentrations (explained in detail through Section 5).

3 Thermochemical behavior of concentrated seawater upon freezing

To accurately model the thermochemical transformation of the brine and formation of ice and salt-hydrate compounds as the brine goes through the freezing process, the OLI Alliance engine for Aspen PLUS is utilized [22,23]. The OLI utilizes the mixed solvent electrolyte model (MSE) that can predict electrolyte behavior from infinite dilution to molten salts. The MSE model is based on readily predicted equilibrium constants and other standard state partial molal thermodynamic properties. The activity coefficient model is based on a Uniquac term, an extended Debye-Huckel term, and a middle-range electrolyte term. The developed integrated ASPEN PLUS + OLI model includes a heat exchanger unit with fixed outlet temperature. The seawater at various levels of concentration is introduced to the heat exchanger. The model determines the chemical composition of the output stream at the prescribed outlet temperature, including the volume fractions of generated ice, salt-hydrates (if any), and the unfrozen concentrated brine. In this study, the typical composition of seawater is used for the feed stream at different concentrations of 35,000 ppm, 50,000 ppm, 75,000 ppm, 100,000 ppm, 150,000 ppm, and 200,000 ppm. The ionic composition of all the investigated brines is that of typical seawater [24] shown in Table 1. Various concentrations are formed by changing the pure H_2O content of this standard composition where the adopted pure water mass fraction values per unit mass of feed are 0.96, 0.95, 0.925, 0.9, 0.85 and 0.8. This is consistent with seawater desalination where the reject brine is created by extracting freshwater from the seawater.

Table 1. Typical ionic composition of seawater [24].

Cl^-	Na^+	SO_4^{2-}	Mg^{+2}	Ca^{+2}	K^{+1}	HCO_3^-
18,980 (ppm)	10,556 (ppm)	2,649 (ppm)	1,262 (ppm)	400 (ppm)	380 (ppm)	140 (ppm)

4 Configuration of direct freeze desalination system

The generalized optimal FD system (direct and indirect) configuration corresponds to the maximum efficiency of the system in terms of the energy used per unit mass of treated water. The maximum efficiency can be achieved by maximizing the coefficient of performance (COP) of the vapor compression cycle providing cooling, and by maximizing the energy recovery form the discharging streams. If the above conditions are satisfied, the theoretical work consumption would closely approach the benchmark theoretical minimum work of separation for work-driven desalination process [21]. According to these criteria, the FD system configuration presented in Fig. 1 can achieve the maximum efficiency by full energy recovery from the ice and discharging streams and maximizing the COP by using a cascade configuration.

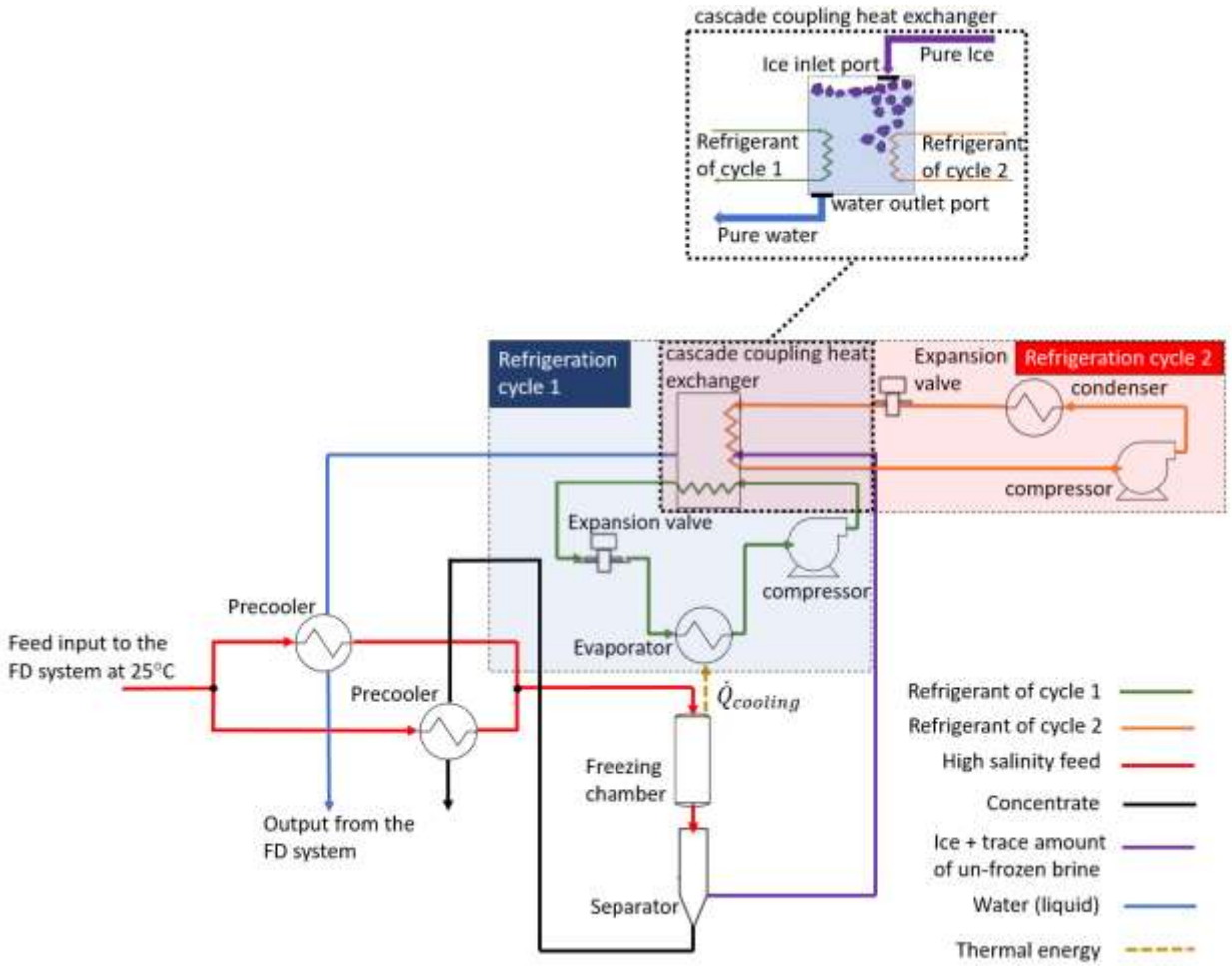

Fig. 1. Optimal freeze desalination system configuration.

For the optimal FD configuration presented in Fig. 1, the inlet feed brine is first precooled (using cooling energy recovered from the return streams), then further cooled down in the freezing chamber to partially freeze. The freezing chamber is cooled by a cascade refrigeration cycle. The stream leaving the freezing chamber is introduced to a separation stage to separate the ice in the slurry from the concentrate (including unfrozen brine and other formed solids). The separated ice may have a percentage of high salinity unfrozen brine encapsulated in pockets within the ice [25-27] (the exact amount of entrapped brine is quantified based on laboratory experiments described later in this section).

The concentrate stream leaving the separator is utilized for precooling the inlet feed brine. The return ice stream is also utilized for cooling energy recovery through melting inside the shell-side of the cascade coupling heat exchanger (explained in the following) and then precooling the inlet feed brine.

4.1 Effectiveness of the separation process

After generating ice in the freezing chamber, it must be separated from the rest of the slurry before being melted. Researchers have used several separation methods for this purpose, including presses, gravity drainage, centrifugal drainage, filter, wash column and sweating ice [28-34]. None of these methods can perfectly separate the unfrozen brine from the ice and in all cases the separated ice will contain some amount of unfrozen brine. This brine is later mixed with the melted ice during melting and degrades the quality of the final treated water. It has been shown that generally the higher the recovery ratio (R), corresponding to lower freezing chamber temperature, the higher the TDS of the treated water [35]. In other words, as the recovery ratio - and the salinity of the rejected unfrozen brine - increases, the quantity of the unfrozen brine contaminating the treated water also increases. In this work, effectiveness of the separation process is approximated using the data obtained from an experimental freeze-desalination prototype developed by the authors [17,36]. The prototype uses a centrifugal draining process to remove the unfrozen brine from the ice. The experimental data showed that the salinity ratio of the treated water to the rejected unfrozen brine, $S_{\mathrm{tw}}/S_{\mathrm{rb}}$, remained almost constant at about 0.02. For any given feed brine salinity and recovery ratio, $S_{\mathrm{tw}}/S_{\mathrm{rb}}$ can be used to find the salinity of the treated water from the following equation:

$$S_{\mathrm{tw}} = \left(\frac{S_{\mathrm{tw}}}{S_{\mathrm{rb}}}\right)\frac{S_f}{1 - R\left(1 - \frac{S_{\mathrm{tw}}}{S_{\mathrm{rb}}}\right)} \tag{1}$$

Equation 1 is obtained from a mass balance of the salt and water through the desalination system (derivation is presented in Appendix B). Considering the experimentally determined salinity ratio of $S_{\mathrm{tw}}/S_{\mathrm{rb}} \approx 0.02$, Eq. 1 is rewritten as:

$$S_{\mathrm{tw}} = \frac{0.02\, S_f}{1 - 0.98\, R} \tag{2}$$

4.2 The cascade coupling heat exchanger

The cascade coupling heat exchanger is a heat exchanger serving as the condenser for the refrigeration cycle 1 and as the evaporator for the refrigeration cycle 2 (Fig. 1). The ice stream leaving the separator is introduced to the shell-side of the cascade coupling heat exchanger to completely melt before leaving as liquid water (schematically illustrated in the excerpt of Fig. 1). The cascade coupling heat exchanger is utilized in the optimal FD system design to provide essential support in raising the system's thermal efficiency. It can be shown that without melting the ice to cool the condenser of refrigeration cycle 1, the cooling capacity of the ice associated with its latent heat of fusion cannot be fully recovered (see Appendix C for proof). Therefore, utilizing the cascade coupling heat exchanger is essential in the optimal configuration of the FD

system to ensure the complete energy recovery from the ice on the return stream side which plays a dominant role in maximizing the FD system's thermal efficiency.

The shell-side temperature of the cascade coupling heat exchanger strongly affects the work consumption of the system [17]. The optimal shell-side temperature of the cascade coupling heat exchanger is the minimum temperature that guarantees full melting of the ice since it enables full recovery of the latent cooling capacity of the ice and provides greater capacity for precooling of the feed brine due to lower temperature of the melted ice. The melting temperature of the separated ice depends on its entrapped brine content. As such, the amount of salt entrapped in the ice affects the optimal shell-side temperature of the cascade coupling heat exchanger. Figure 2 (corresponding to feed salinity of 35,000 ppm, freezing chamber temperature of -35°C, and ambient temperature of 25°C) indicates the minimum condenser shell-side temperatures that allow for the complete melting of ice at different unfrozen brine mass fractions (the mass ratio of the liquid brine in the ice stream to the total mass of the ice stream). For a theoretical case of perfect ice separation (no liquid brine entrapped within the ice stream), the optimal cascade coupling heat exchanger shell-side temperature is 0°C. Higher quantities of the unfrozen brine (carried over in the return ice stream) are linked to lower recovery ratios (higher freezing temperatures) and vice versa. This explains the temperature trend in Fig. 2 having a relatively higher slope at lower brine mass fractions. In the case of higher freezing temperatures, the lower mass of formed ice along with the corresponding higher quantities of unfrozen brine (carried over within the return ice stream) allows the melting of the ice at relatively lower intermediate condenser temperatures due to the relatively higher overall concentration of the return stream (more high salinity brine and less ice). On the other hand, in the case of lower freezing temperatures (higher recovery ratios), the higher mass of formed ice and lower quantities of unfrozen brine make it necessary to reach higher temperatures for the complete melting of ice due to the lower overall concentration.

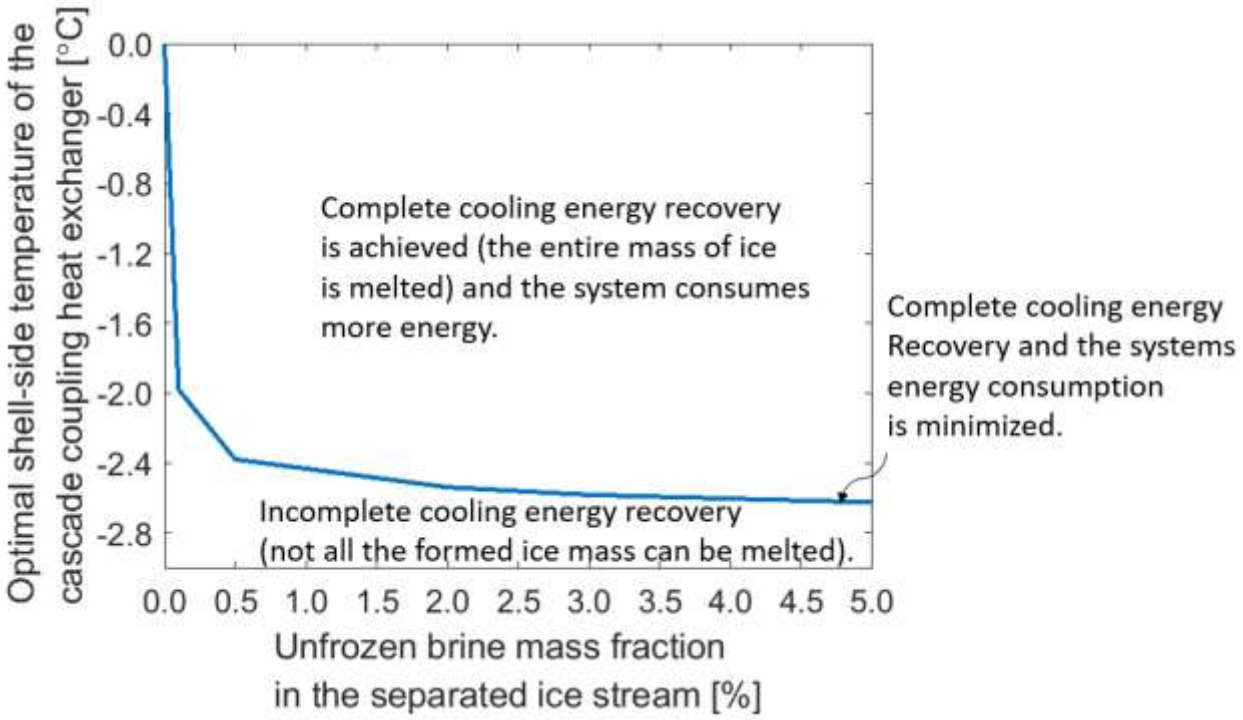

Fig. 2. Optimal shell-side temperature of the cascade coupling heat exchanger for various unfrozen brine mass fractions in the return ice stream (obtained for feed salinity of 35,000 ppm, freezing chamber temperature of -35°C, and ambient temperature of 25°C).

5 Thermochemical modeling of the freeze desalination system

A freeze desalination system model should cover the brine thermochemical transformation as it goes through freezing and melting processes in the system. The model should also predict thermal performance and work consumption of the process for various feed qualities and recovery ratios.

The following assumptions are adopted in developing the freeze desalination model:

- The analysis is conducted under the assumption of a steady-state condition.
- The effectiveness of heat transfer within the system's evaporator, condenser and cascade coupling heat exchanger is represented by a temperature difference ΔT between the hot and cold media reported in the literature [37] (detailed in Section 4.1).
- An inert water-immiscible intermediate cooling liquid (ICL) circulates between the evaporator of the refrigeration cycle 1 and the freezing chamber to cool the feed brine.

- Well-mixed slurry at the outlet of the freezing chamber; the ice, unfrozen brine, possible salt-hydrates, and the ICL are at thermal equilibrium.
- All phases are presumed to be in a state of equilibrium throughout the analysis.
- Negligible heat gain/loss from/to the ambient.

5.1 Refrigeration cycles model

The optimal freeze desalination cycle configuration is composed of a two-level cascaded refrigeration cycle [17]. The *T*-*s* diagram for each of the two cycles is presented in Fig. 3, where the transition of the refrigerant state from 1 to 2 results from irreversible compression. Constant pressure heat rejection occurs from state 2 to 3. Isenthalpic expansion occurs from state 3 to 4 and constant pressure heat addition takes place from state 4 to 1. The model accounts for the two dominant sources of irreversibility in vapor compression refrigeration cycles, namely the compression isentropic efficiency, and heat transfer effectiveness of the heat exchangers.

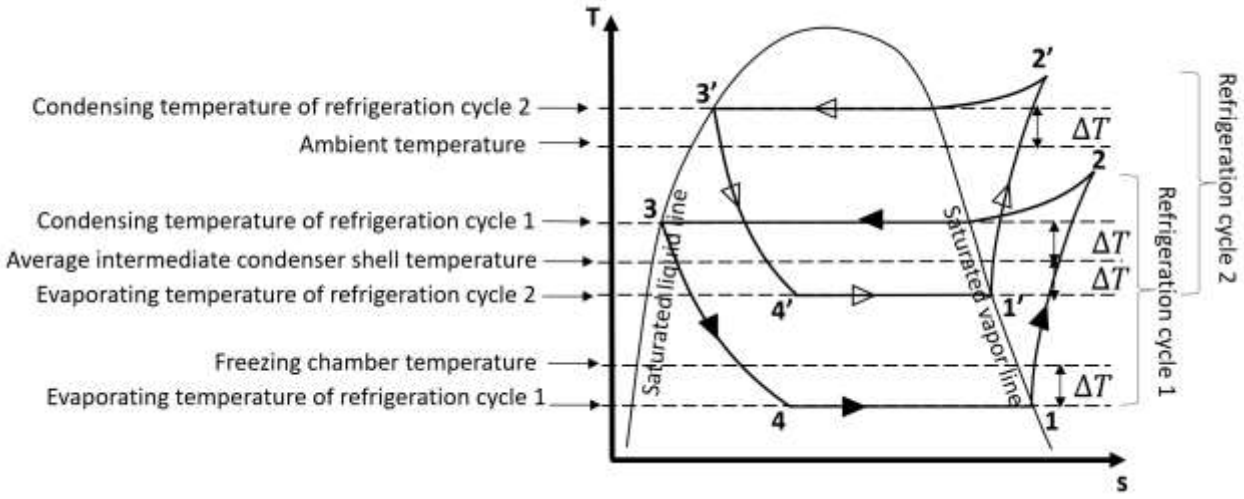

Fig. 3. The *T*-*s* diagram corresponding to each of the two refrigeration cycles utilized in the optimal configuration freeze desalination system.

The variation in heat transfer effectiveness is modeled by applying a temperature difference between the two fluids in each of the systems' primary heat exchangers [37]. As shown in Fig. 1, the studied freeze desalination system is composed of three primary heat exchangers: the evaporator, the condenser, and the cascade coupling heat exchanger. The temperature difference corresponding to variation in heat transfer effectiveness is applied as described in Figs. 3. Figure 3 also shows the evaporating temperature of refrigeration cycle 1 below the desired ICL temperature (the temperature desired for the ICL to reach at the outlet of the evaporator) by a designated temperature difference, ΔT. Similarly, the condensing temperature of refrigeration cycle 2 is above the ambient temperature by a designated temperature difference, ΔT.

The shell-side temperature of the cascade coupling heat exchanger is maintained at the optimal temperature described in Section 4.2. In addition, Fig. 3 shows the evaporating and condensing temperatures corresponding to the refrigeration cycles 2 and 1, respectively, relative to the cascade coupling heat exchanger shell-side temperature. To account for the irreversibility of the compression process, the compressor's isentropic efficiency is calculated using the following two equations for refrigeration cycles 1 and 2, respectively.

$$\eta_{isentropic,1} = \frac{h_{2s} - h_1}{h_2 - h_1} \times 100\% \tag{3}$$

where, h_1 and h_2 are the refrigerant's enthalpy at points 1 and 2, respectively, and h_{2s} is the refrigerant outlet enthalpy under ideal isentropic compression.

$$\eta_{isentropic,2} = \frac{h_{2's} - h_{1'}}{h_{2'} - h_{1'}} \times 100\% \tag{4}$$

Similar to Eq. 3, $h_{1'}$ and $h_{2'}$ represent the enthalpy at points $1'$ and $2'$, respectively, and $h_{2's}$ represents the refrigerant outlet enthalpy under ideal isentropic compression.

Considering the operating temperatures in this system, R404A is the selected refrigerant for both refrigeration cycles and its thermodynamic properties are obtained using the CoolProp package [38]. Note that the system performance using other refrigerants shows a deviation of less than 5% compared to the refrigerant R404A.

5.2 Co-simulation of integrated FD system model

The freeze desalination system behavior and performance are analyzed through co-simulation of the component models as illustrated in Fig. 4. The significance of adopting this approach is that it allows for the extrapolation of results beyond the available experimental points used to validate the framework (validation presented in Section 6). A master code orchestrates the simulation of the feed thermo-chemical properties in ASPEN PLUS + OLI engine along with the cascade refrigeration cycles model. In the following subsections, the three main blocks of the co-simulation framework (MATLAB master code, refrigeration model and ASPEN PLUS OLI suite) are described in detail.

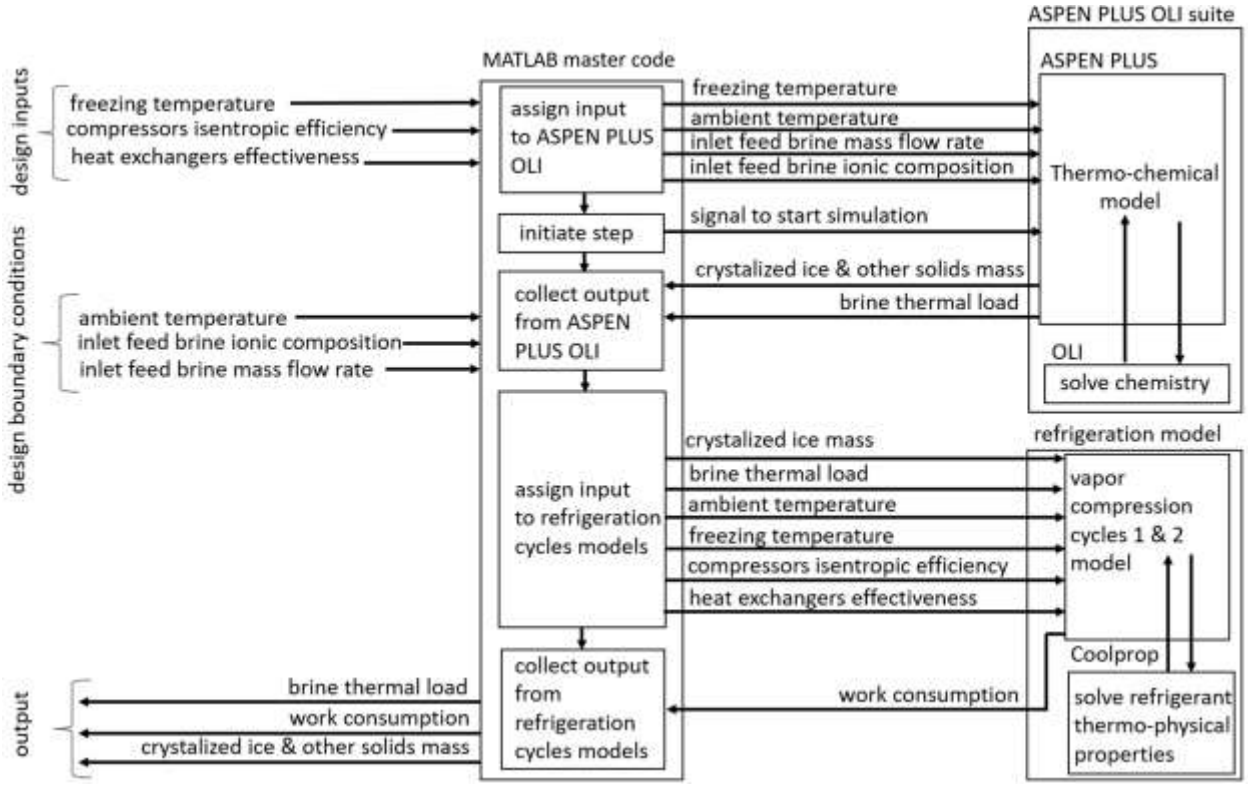

Fig. 4. Layout of the co-simulation framework developed in this study.

5.2.1 Master code of the co-simulation framework

The master code running the co-simulation framework is written in MATLAB. The code establishes a connection with ASPEN PLUS, assigns input, runs the ASPEN simulation file for a specified period then collects the output. The master code also utilizes MALTAB functions for estimating the cascade refrigeration cycle performance. Figure 5 shows the detailed structure of the framework's master code.

MATLAB master code

```
% Link MATLAB with ASPEN PLUS
Aspen = actxserver('Apwn.Document.39.0');
% Get attributes of folder (necessary to establish the location of the simulation
folder) and assign simulation file name
[stat,mess] = fileattrib;
Sim_Name = 'file1';
Aspen.invoke('InitFromArchive2',[mess.Name '\' Sim_Name '.bkp']);
% Identify the ASPEN PLUS window and dialogues visibility
Aspen.SuppressDialogs = 1;
Aspen.Visible = 0;
% Run simulation
Aspen.Engine.Run2(1);
% Assign inputs
    % Example of input assignment:
    Aspen.Tree.FindNode("\Data\Blocks\CLR1A\Input\TEMP").value = temperature_value_assigned;
                                  % Call to variable in ASPEN
% Initiate, run & stop ASPEN simulation
Aspen.Reinit;
Aspen.Engine.Run2(1);
time = 1;
while Aspen.Engine.IsRunning == 1
    pause(0.5);
    time = time+1;
    if time == desired_simulation_stop_time
        Aspen.Engine.Stop;
    end
end
% Collect outputs
    % Example of output collection:
    load_value_collected = Aspen.Tree.FindNode("\Data\Blocks\COOLER\Output\QCALC").value;
% Utilize refrigeration cycle model using MATLAB functions
[outputs_from_function] = refrigeration_cycles_model(inputs_to_function);
% Save output
save('data_file_name.mat','variable1', ,'variable2', ,'variable3',.....)
```

Fig. 5. MATLAB master code of the co-simulation framework.

5.2.2 Refrigeration model application in the co-simulation framework

The refrigeration cycles model described in Section 5.1 is utilized to estimate its energy performance as part of the integrated FD system model. The evaporating temperature of refrigeration cycle 1 is less than the temperature inside the freezing chamber by the heat exchanger's approach temperature, ΔT (as described in Section 5.1, the variation in heat transfer effectiveness is modeled by applying a temperature difference between the two fluids in each of the systems' heat exchangers). Equation 5 represents the evaporating temperature for refrigeration cycle 1. Similarly, the condensing temperature for refrigeration cycle 2 is higher than the ambient temperature by the heat exchanger's approach temperature, ΔT as shown in Eq. 6. The evaporating temperature of refrigeration cycle 2 is lower than the cascade coupling heat exchanger shell side temperature by the exchanger's approach temperature, ΔT while the condensing temperature of refrigeration cycle 1 is higher than the shell side temperature by ΔT. The compression irreversibility is counted for using the isentropic efficiency values calculated by Eq. 3 and 4.

$$T_e = T_{ch} - \Delta T \quad (5)$$

$$T_c = T_a + \Delta T \quad (6)$$

The evaporating load of refrigeration cycle 1 required to cool the brine down to the desired temperature inside the freezing chamber is the product of the refrigerant mass flow rate and the difference between the enthalpies at the exit and inlet of the evaporator as presented in Eq. 7.

$$Q_e = m_r\,(h_{e,o} - h_{e,i}) \quad (7)$$

The condensing heat and the work of each of the two compressors are estimated using Eq. 8 and 9 respectively.

$$Q_c = m_r\,(h_{c,i} - h_{c,o}) \quad (8)$$

$$W_{comp} = m_r\,(h_{comp,o} - h_{comp,i}) \quad (9)$$

The evaporating load of refrigeration cycle 2 handles the condensing heat of refrigeration cycle 1 minus the cooling energy recovered from melting the ice inside the intermediate condenser shell as shown in Eq. 10.

$$Q_e = Q_c - Q_m \quad (10)$$

The overall work requirement of the FD system is the sum of the work of each of the system's compressors.

5.2.3 ASPEN PLUS OLI suite description

As described briefly in Section 3, the utilized ASPEN PLUS + OLI model includes a heat exchanger unit with fixed outlet temperature where the mixed solvent electrolyte model (MSE) of OLI is adopted to predict the brine's thermochemical behavior. In the following subsections, the ASPEN PLUS and the OLI models are described in more detail.

5.2.3.1 ASPEN PLUS model

The ASPEN PLUS model consists of a heat exchanger and a separator as shown in Fig. 6. The adopted seawater composition (ionic composition defined in table 1) is configured in the ASPEN PLUS model and utilized for the input seawater brine stream (S1). The input stream is then logged to a separator that removes a certain amount of liquid H_2O from the stream. The removal of H_2O (S2) raises the mixture's salinity and enables modeling different concentrations of the high salinity brine feed to the FD system (S3), namely, 35,000 ppm, 50,000 ppm, 75,000 ppm, 100,000 ppm, 150,000 ppm, and 200,000 ppm. The brine feed is cooled down to the freezing chamber temperature assigned by the master code. The thermal load and the chemical behavior of the brine is calculated using OLI (explained in more detail through the following subsection). The thermal load associated with the process and the chemical composition of the product stream are collected by the master code. Similarly, the cooling energy recovered inside the cascade coupling heat exchanger and through the precooling process is counted for in the calculations of the master code using data generated by an ASPEN PLUS model coupled with OLI.

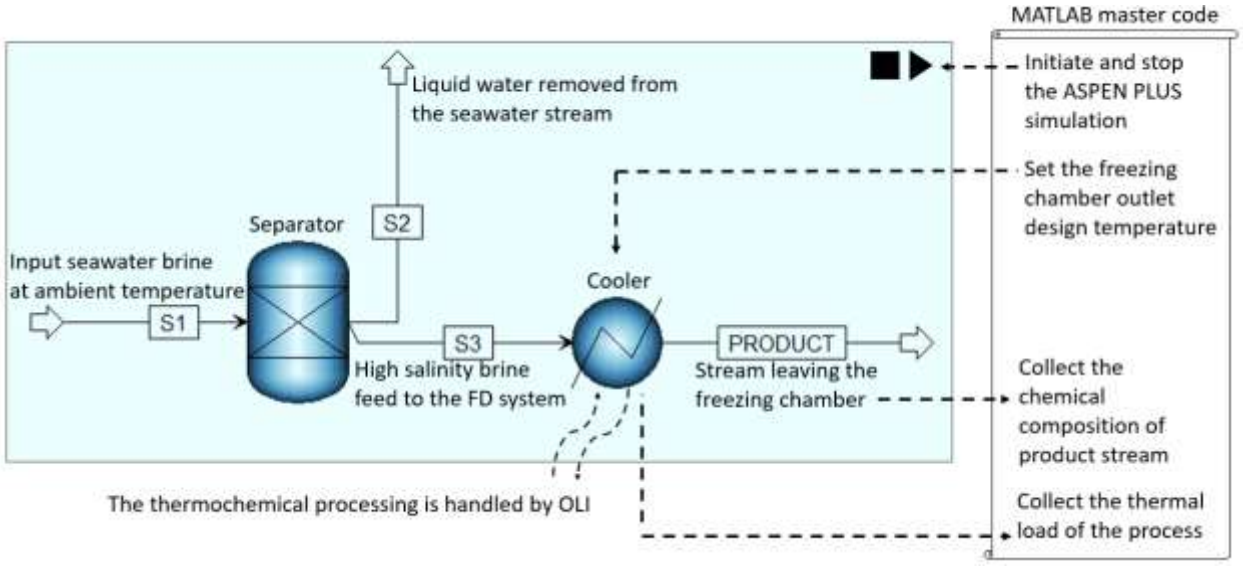

Fig. 6. ASPEN PLUS model.

5.2.3.2 OLI model

As described briefly in Section 3, OLI utilizes the mixed solvent electrolyte model (MSE) which represents the chemical and phase equilibria in addition to the volumetric and thermal properties for mixed solvent electrolyte systems from infinite dilution to molten salts [39]. The MSE model has been extensively validated against experimental data [39-49]. The experimental data utilized to determine the MSE model parameters included the heat capacities, the densities, the Gibbs energy of transfer of electrolytes, the heats of mixing and dilution, the osmotic coefficients in aqueous solutions, the acid dissociation constants as a function of the solvent composition, the solubility of salts, and the activity coefficients in completely dissociated aqueous systems [39].

The electrolyte solution nonideal behavior is affected primarily by the electrostatic (long-range) effects due to the electric charges of the ionic species [39,50,51], the physical dispersion forces and structural differences between the species [39,52,53], and the chemical forces chemical forces leading to complex formation or association [39]. To consider the described effects, the MSE model combines the excess Gibbs energy expression with chemical equilibrium relations. The chemical equilibrium calculations involve the simultaneous use of the standard state thermodynamic properties (linked to the species engaging in the chemical reactions) and activity coefficients [39]. The excess Gibbs energy and the activity coefficient expressions adopted by the MSE model are presented in Eq. 11 and 12, respectively. For the MSE model, comprehensive data has been published about the selection of the reference state and the standard state chemical potentials conventions [39]. The published work included detailed information about the long, the short and the middle range interaction contribution as well as density, enthalpy and heat capacity calculations [39].

$$\frac{G}{R_g T_K} = \frac{G_L}{R_g T_K} + \frac{G_M}{R_g T_K} + \frac{G_S}{R_g T_K} \qquad (11)$$

$$ln\gamma = ln\gamma_L + ln\gamma_M + ln\gamma_S \qquad (12)$$

Where G_L is the contribution of the long-range electrostatic interactions, G_M is the contribution of the middle range ionic interactions, and G_S represents the short-range contribution resulting from ion/ion, molecule/molecule and molecule/ion interactions. Similarly, γ_L, γ_M and γ_S are the activity coefficients linked to the long, medium and short-range interactions.

6 Results

The results are presented in two parts: part 1 presents, the cooling load required for freezing of standard and concentrated seawater at different temperatures and the correspondingly formed compounds along a temperature range of -35°C to 0°C. Part 2 is dedicated to the FD system's work consumption considering the effects of the compressors' isentropic efficiency and effectiveness of the primary heat exchangers.

6.1 Brine's cooling load of freezing and threshold of formation of various compounds

The thermochemical model described in Section 2 is validated by comparing the ice recovery ratio values with the previously reported experimental data for standard and concentrated seawater presented in Fig. 7 [54]. The maximum error between the model predictions and the actual measurements is less than 5% for concentrations of 35,000, 50,000 and 75,000 ppm. For the concentrations of 100,000 ppm and 150,000 ppm, the maximum error is within the 10% margin. In the case of the 200,000 ppm feed salinity, the estimated values lie within a 25% error margin, with the theoretical results overpredicting the mass of formed ice compared to the experimental data. The relatively large error for TDS of 200,000 ppm is possibly due to the difficulty of the complete separation of the ice from the formed hydrohalite ($NaCl \cdot 2H_2O$) in the experimental studies which is exacerbated at higher brine salinities.

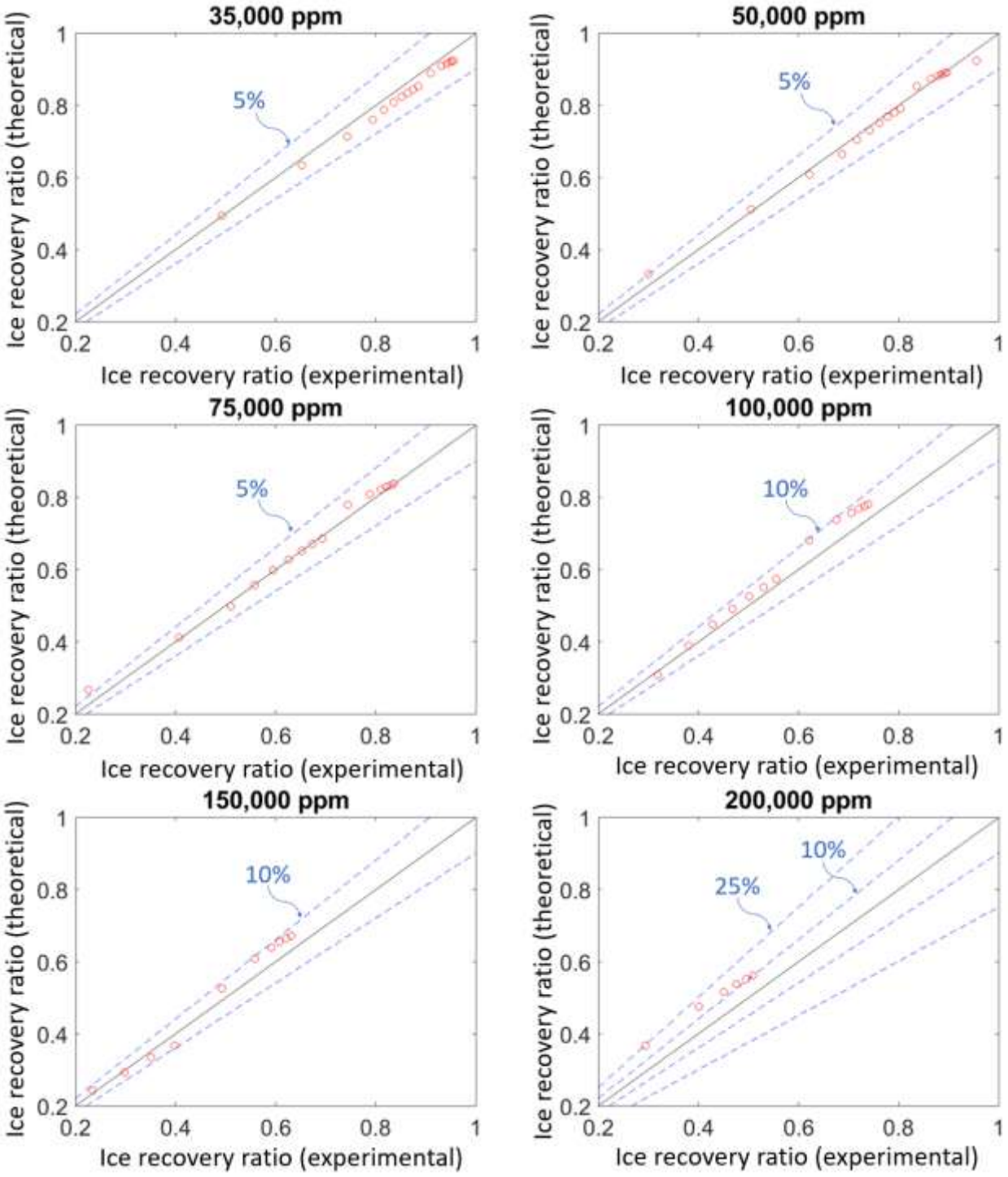

Fig. 7. Theoretical ice recovery ratio vs. experimental values.

Utilizing the validated model to predict the ice mass fractions for the different feed concentrations at different freezing temperatures, a phase diagram presented in Fig. 8 is generated to highlight the input stream, output stream and the onset of freezing within the FD system.

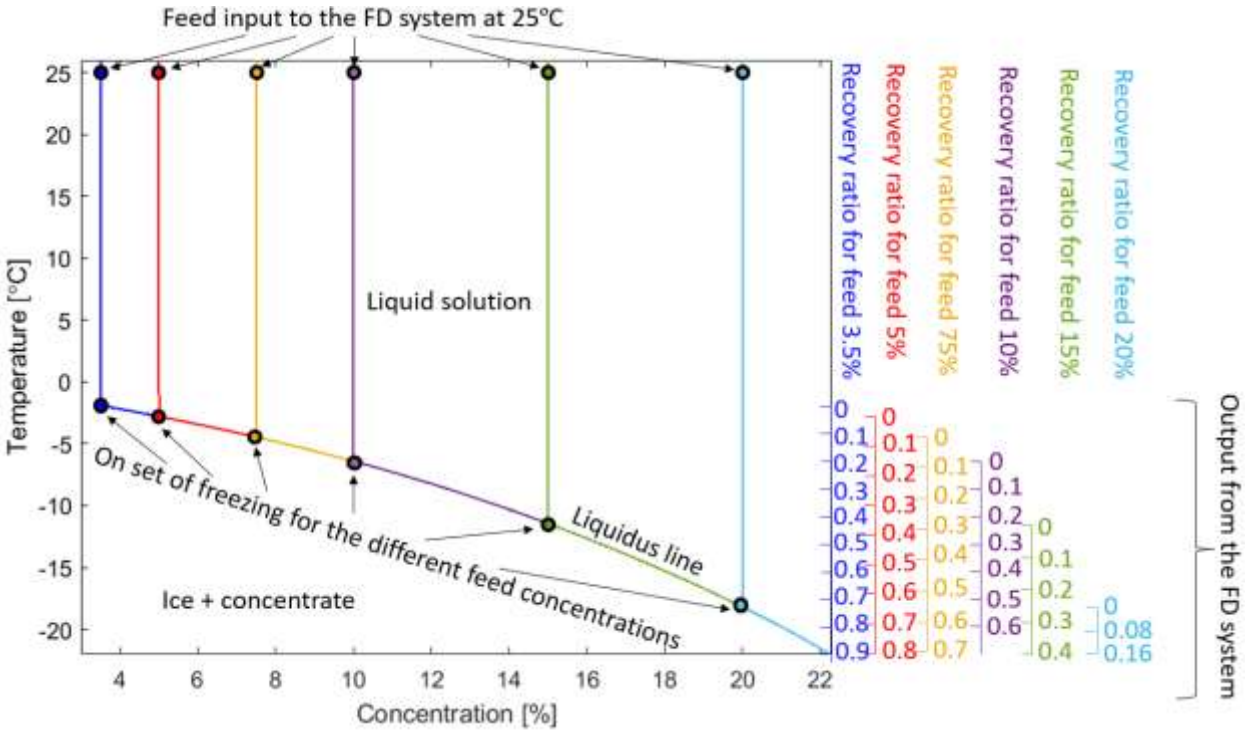

Fig. 8. Phase diagram for seawater feed at different concentrations.

Upon freezing, the brine is decomposed into four main components, namely, unfrozen brine (will be referred to as brine), pure ice, hydrohalite and solids (salt-hydrates and other suspended solids). Figure 9 shows the mass fraction of each of these components at various temperatures for standard and concentrated seawater.

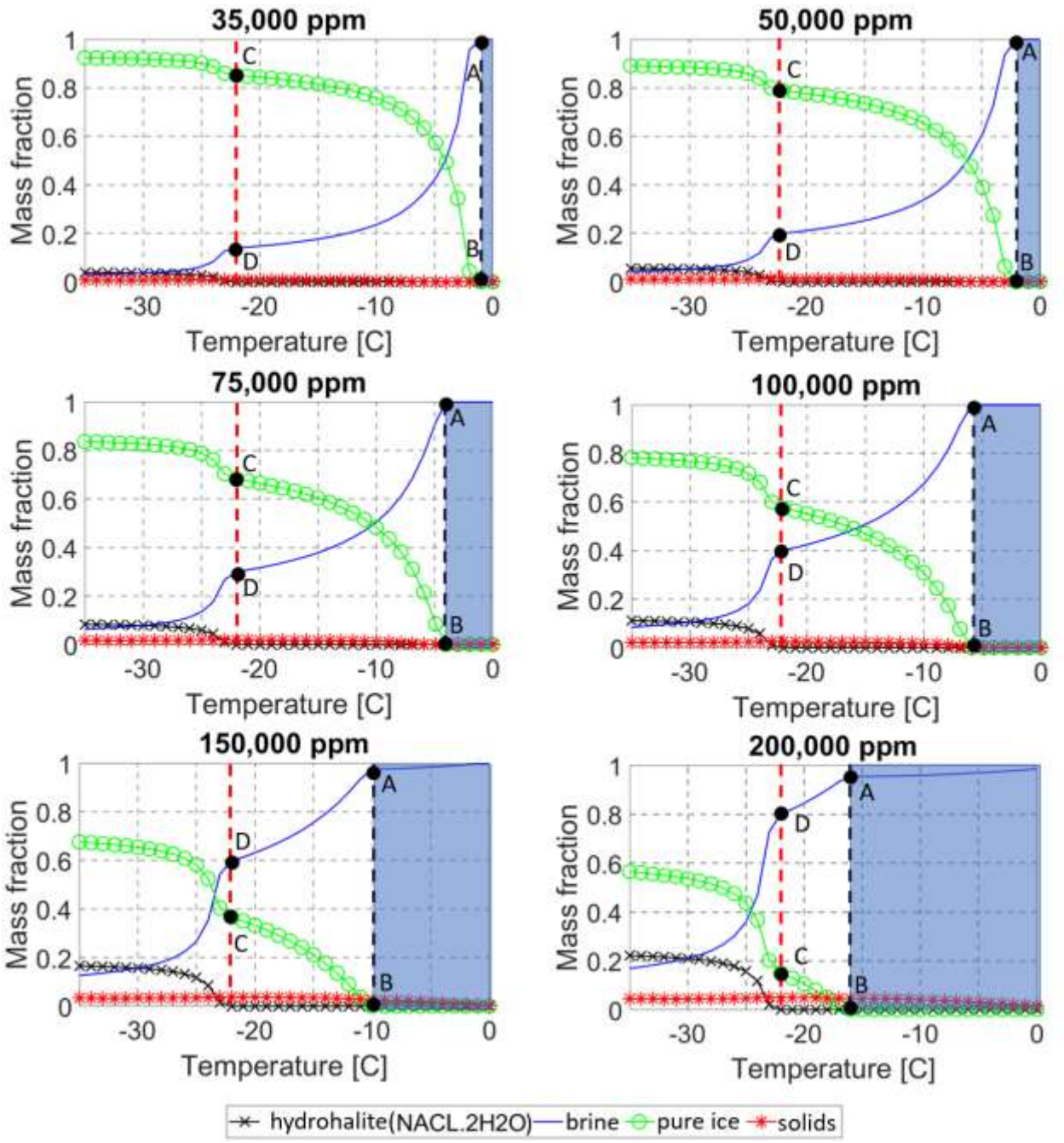

Fig. 9. Mass fractions of various components formed upon cooling of standard and concentrated seawater between 0°C and -35°C.

In Fig. 9, the brine refers to liquid phase containing water and dissolved ions. Three regions can be identified in Fig. 10, separated by two vertical dashed lines, namely line AB connecting points A and B, and line CD connected points C and D. Line AB shows the onset of freezing, where the first ice crystals are formed, and line CD shows the onset of hydrohalite formation. In an analogy with a binary NaCl-water solution, line CD is equivalent to the eutectic temperature. It

is noted, however, that due to its diverse composition, seawater does not have a single eutectic temperature. As evident in Fig. 8 and 9, the onset of freezing temperature is suppressed significantly as the brine TDS increases; decreasing by almost 15°C as the brine TDS increases from 35,000 ppm to 200,000 ppm. On the other hand, the formation temperature of hydrohalite remains almost constant at about -23°C for various brine salinities, that is consistent with previous studies [55].

In the region to the right of line AB, there is no ice, and the mixture is primarily composed of liquid and small amounts of solids that start to precipitate below 0°C. In the middle region, between lines AB and CD, ice, brine, and some solids are present. Further cooling in this region leads to an increasing amount of ice and decreasing amount of brine with no noticeable change in the amount of precipitated solids. In the region to the left of line CD, hydrohalite is added to the mixture.

Figure 9 also shows that the higher the concentration of the feed brine, the higher the temperature at which solids precipitation commences. In addition, for temperatures lower than -23°C, the mass fraction of hydrohalite is higher for higher feed salinities. The higher mass fraction of solids and hydrohalite is explained by the mixture saturation occurring at higher temperatures for higher concentration feed brine.

Reducing the temperature below the formation threshold of hydrohalite induces a sharp rise (drop) in both the ice and hydrohalite (liquid brine) mass fraction. These significant changes near ~ -23°C can be explained by the fact that the Na^+ and Cl^- ions largely dominate the ionic composition of the brine. Therefore, the behavior of the brine near -23°C is very similar to the behavior of binary NaCl-H_2O system near -21.1°C where it undergoes eutectic freeze with no leftover liquids.

The specific cooling load is the amount of cooling energy required to generate 1 kg of purified water, in the form of ice, by removing sensible and latent heat from the brine. Figure 10 shows the specific cooling load of the feed brine starting at 0°C cooled down to different temperatures below the threshold of freezing. The effect of the supercooling phenomenon has been considered in the cooling load analysis. The outcomes presented in Fig. 10 are based on supercooling of 0.383 ºC (below the threshold of freezing) for the different feed concentrations. At the same freezing temperature, the higher the feed concentration, the lower the mass of the ice crystallized (compared to lower feed concentration) as described earlier (Fig. 9).This explains the higher cooling load per kg of crystallized ice in the case of higher feed concentrations. Also at higher concentrations, the cooling load (per kg of crystallized ice) decreases at lower freezing temperatures. This is linked to the higher recovery ratio values where a larger portion of the cooling energy (provided to reach the desired freezing temperature) is consumed to crystallize ice rather than sensibly cool high salinity unfrozen brine.

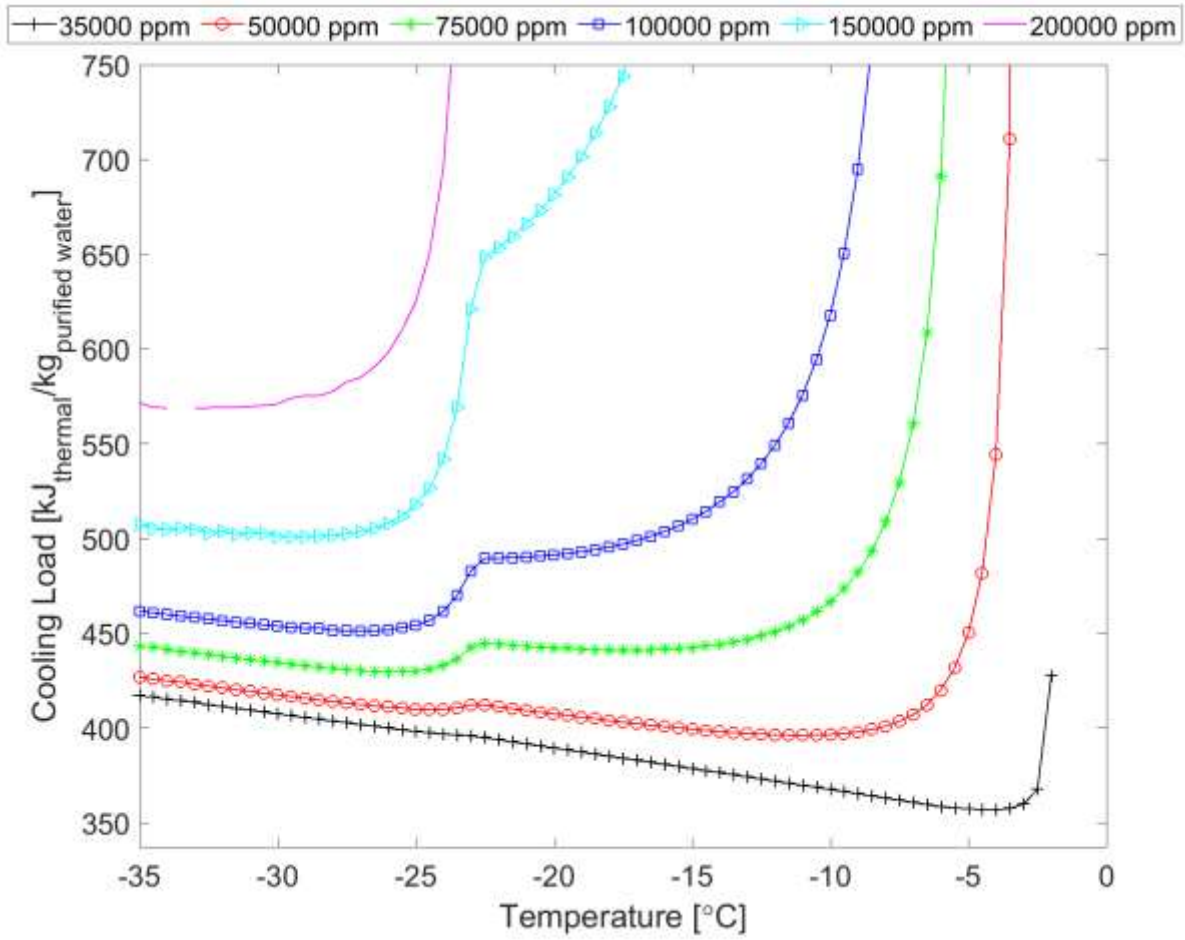

Fig. 10. Brine specific cooling load at different freezing temperatures for various feed concentrations.

6.2 Freeze desalination system's work consumption

The freeze desalination system's specific work is the amount of work consumed by the system to generate 1 kg of purified water. The minimum possible specific work of separation (separation of water from the feed brine) corresponds to a water recovery ratio (mass ratio of the purified water to the saline feed water) approaching zero as proved in published studies [56,57]. From Fig. 10, as the water recovery ratio approaches zero ($R \rightarrow 0$), the freezing chamber temperature approaches the onset of freezing for each feed concentration. Therefore, the desalination minimum work of separation corresponds to temperatures approaching the start of freezing for each feed concentration as presented in Eq. (4).

$$\mathrm{SWFD_{min}} \equiv \lim_{T_{\mathrm{ch}} \rightarrow T_{\mathrm{fz}}} \mathrm{SWFDW} \tag{5}$$

where SWFD is the specific work of freeze desalination corresponding to various feed concentrations and brine freezing chamber temperatures, T_{ch} and T_{fz} are the temperatures inside the freezing chamber and the freezing temperature for each of the feed concentrations, respectively.

To validate the proposed FD system's configuration in terms of minimizing the work of separation for desalination, the proposed system's model has been simulated adopting Carnot cycle (for the purpose of comparison with the published benchmark theoretical work of separation values [21]). The theoretically estimated FD work consumption showed agreement with the established values of theoretical work of separation [21] within $\pm 5\%$ error range. Figure 13 shows the theoretically determined work of the FD system (estimated at perfect isentropic efficiency of the system's compressors) compared to the published work of separation values at different water recovery ratios corresponding to inlet seawater salinity of 35,000 ppm and ambient temperature of 25°C. As illustrated in Fig. 11, the published minimum work of separation for desalination of a 35,000 ppm seawater inlet feed at an ambient temperature of 25°C is $2.71\ kJ/kg_{pure\ water}$. The source of error between the published value and the estimated value of the minimum work of separation results from the computational limitation of the utilized ASPEN PLUS + OLI engine that did not converge at recovery ratio values lower than 0.045. Another source of error that also applies to estimations at recovery ratios higher than 0.045 arises from the sources of irreversibility in the system that include the mixing of streams at various temperatures as well as the counter flow heat transfer that occurs at non-zero temperature difference between the two streams (where error between the estimated and the published values lie within $\pm 5\%$ range).

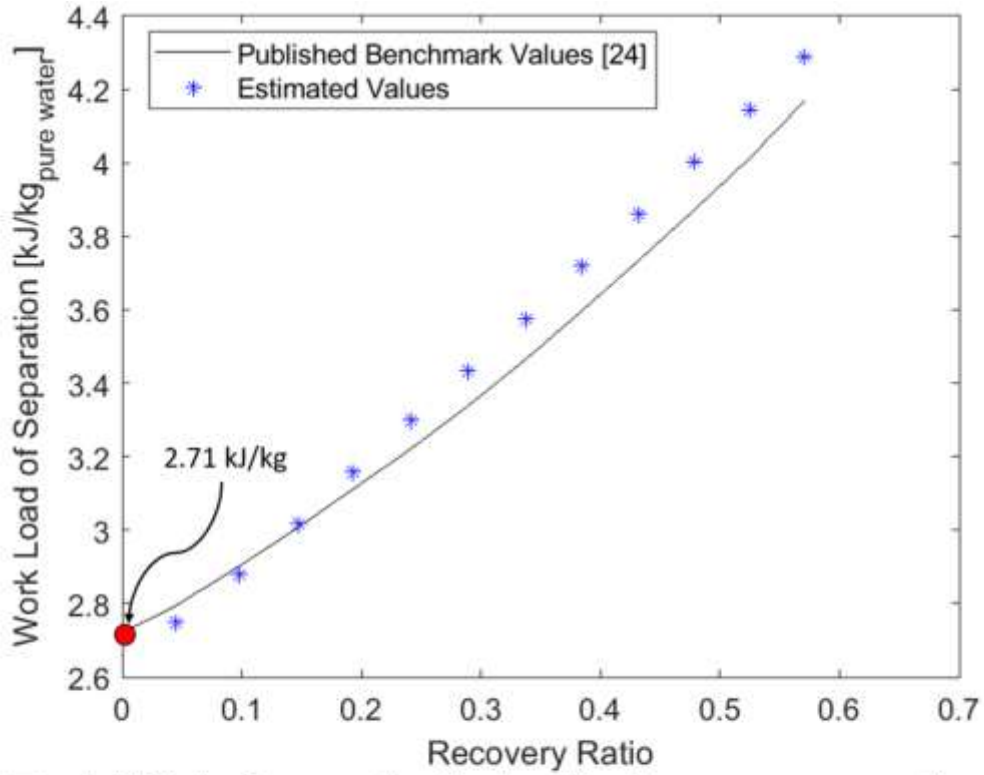

(a) Work of separation for desalination vs. recovery ratio

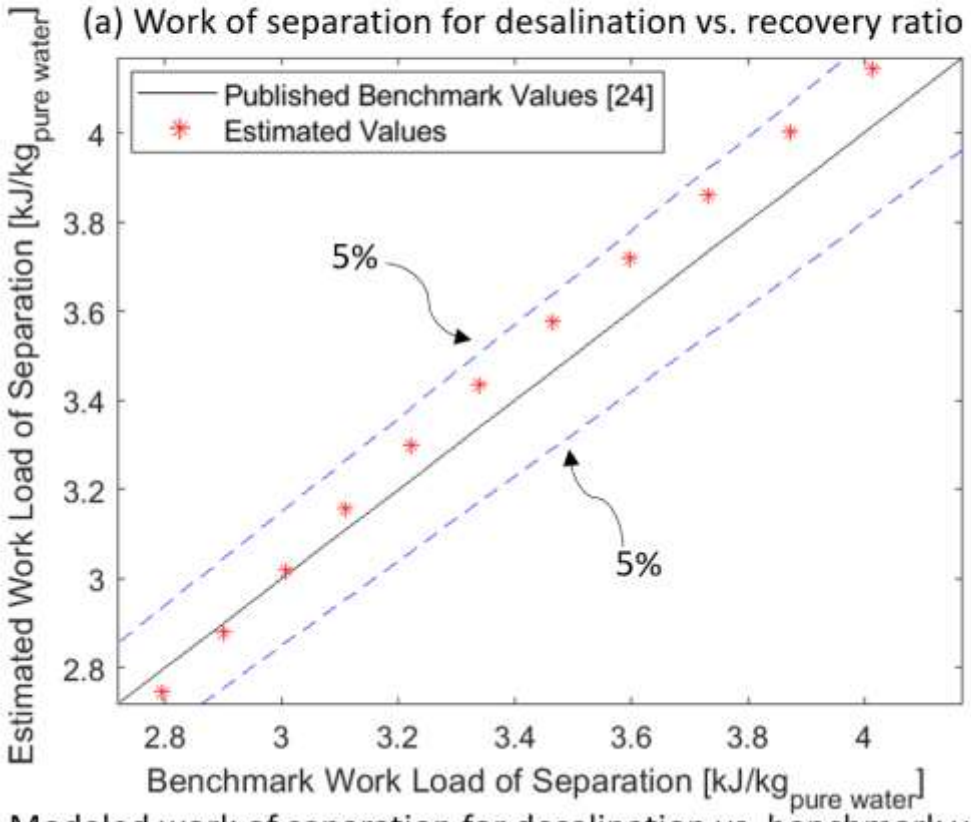

(b) Modeled work of separation for desalination vs. benchmark values

Fig. 11. Estimated work of separation compared to the benchmark theoretical work of separation for desalination [21].

Since the minimum work of separation is achieved as $R \rightarrow 0$, the maximum energy efficiency of the FD system will be achieved at the onset of freezing for any brine concentration. Figure 12 shows the effect of compressor isentropic efficiency on the FD system minimum work of separation for different feed concentrations and heat exchangers' approach temperature, ΔT. As noted, $\Delta T = 0$ corresponds to an isentropic heat exchanger with an effectiveness of 1 and larger ΔT values represent larger irreversibilities and smaller effectiveness values.

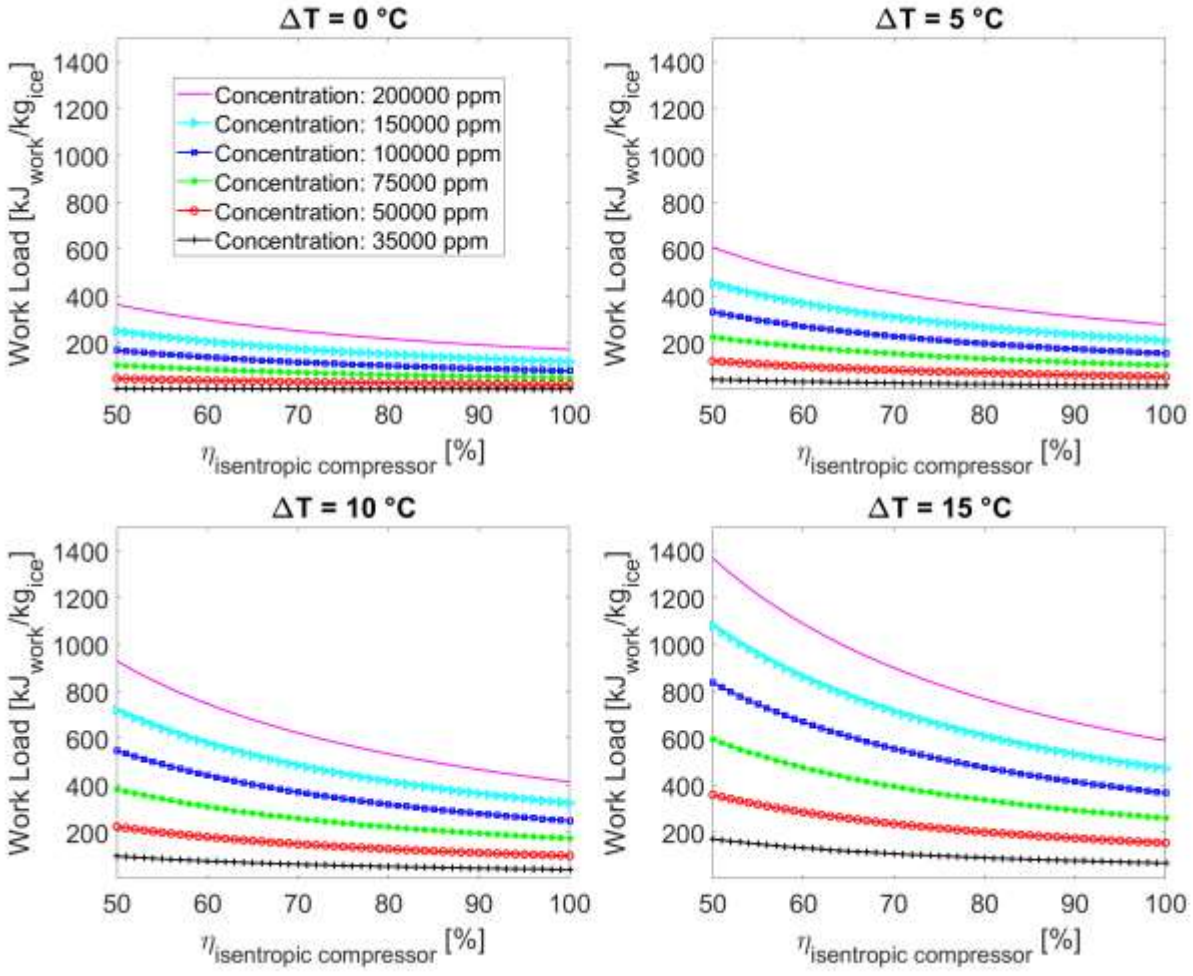

Fig. 12. The minimum work of separation of the freeze desalination system at different concentrations versus compressors' isentropic efficiency for different heat exchanger approach temperatures.

As expected, Fig. 12 shows that the minimum work of separation of the FD system decreases for all feed concentrations as the isentropic efficiency of the system's compressor increases. Also, the lower the heat transfer effectiveness of the system's heat exchangers (higher ΔT values), the

greater the minimum work of separation is. These results also show that the higher the feed concentration, the higher the specific work. The lower intermolecular forces among the molecules of the solvent at higher feed concentrations makes it more energy demanding to freeze the water content within the mixture compared to less concentration feeds. In the case of imperfect salt separation, the work load of the FD system was found to be lower (compared to the perfect salt separation case) which complies with the published entropy-based analysis outcomes [56]. The reduced work consumption comes at the penalty of lower water quality which defies the purpose of desalination.

7 Conclusion

The present study devised a thermochemical model for a FD system configuration capable of achieving maximum efficiency in terms of power consumption per unit mass of treated water. The model comprised a co-simulation framework combining state-of-the-art tools to simulate the thermochemical behavior of the brine upon freezing and the FD system's thermal performance. For a feed salinity of 35,000 ppm, the theoretical work of separation of the investigated FD system configuration ranged from 2.748 $kJ_{work}/kg_{pure\ water}$ to 4.287 $kJ_{work}/kg_{pure\ water}$, corresponding to ice recovery ratios of 0.045 to 0.57. The effect of the isentropic efficiency of the compressors and effectiveness of the primary heat exchangers on the work of desalination were also investigated. The study findings and contributions can be summarized in the following points:

- Proposing a FD system configuration that maximizes energy efficiency. The claim is verified through the proximate between the system's theoretical work of separation with the published benchmark minimum work of separation for desalination.
- A co-simulation framework to simulate the thermochemical behavior of the brine upon freezing and the FD system's thermal performance.
- Comprehensive maps documenting the effect of isentropic efficiency of compressor and heat exchanger effectiveness on the energy performance of the FD system.

The contributions of this study present a reference for selection, sizing, operation and techno-economic analysis of FD systems. As described throughout the paper, this study identifies the optimal FD system configuration and analyzes its energy performance, yet the ability to identify the practical optimal operational freezing chamber temperature resembles a limitation. This results from the effect of other factors on the economics of the FD system besides the energy consumption. The future directions to take for practically implementing the FD system include studying the control of the freezing chamber temperature and investigating the effect of the electricity price, the brine disposal price and the water selling price on the FD system's economics.

Acknowledgement

Support from the Advanced Research Projects Agency-Energy (ARPA-E) under Award Number DE-AR0001069 is acknowledged and appreciated.

References

[1] UN-Water Technical Advisory Unit. Summary progress update 2021: Sdg 6 — water and sanitation for all, July 2021.

[2] The State of Food and Agriculture 2020.Overcoming water challenges in agriculture. Rome. FAO, 2020.

[3] Burek, P., Satoh, Y., Fischer, G., Kahil, M., Scherzer, A., Tramberend, S., Nava, L., Wada, Y., Eisner, S., Fl¨orke, M, Hanasaki, N., Magnuszewski, P., Cosgrove, B., Wiberg, D.. Water futures and solution-fast track initiative. 2016.

[4] Gude, V. G.. Desalination and water reuse to address global water scarcity. Reviews in Environmental Science and Bio/Technology, 16(4), 591-609, 2017.

[5] Panagopoulos, A.. Water-energy nexus: desalination technologies and renewable energy sources. Environmental Science and Pollution Research, 28(17), 21009-21022, 2021.

[6] Micari, M., Moser, M., Cipollina, A., Tamburini, A., Micale, G., & Bertsch, V.. Towards the implementation of circular economy in the water softening industry: A technical, economic and environmental analysis. Journal of Cleaner Production, 255, 120291, 2020.

[7] Kaplan, R., Mamrosh, D., Salih, H., Dastgheib, S.. Assessment of desalination technologies for treatment of a highly saline brine from a potential CO2 storage site. Desalination,404:87-101, 2017.

[8] Tow, E., Warsinger, D., Trueworthy, A., Swaminathan, J., Thiel, G., Zubair, S., Myerson, A., and Lienhard V, J.. Comparison of fouling propensity between reverse osmosis, forward osmosis, and membrane distillation. Journal of Membrane Science, 556:352–364, 2018.

[9] Palacin, L., Tadeo, F., Elfil, H., Prada, C., and Salazar, J.. New dynamic library of reverse osmosis plants with fault simulation. Desalination and Water Treatment, 25(1-3):127–132, 2011.

[10] Jiang, S., Li, Y., Ladewig, B.. A review of reverse osmosis membrane fouling and control strategies. Science of The Total Environment, 595:567– 583, 2017.

[11] Onishi, V. C., Carrero-Parreno, A., Reyes-Labarta, J. A., Fraga, E. S., Caballero, J. A. Desalination of shale gas produced water: A rigorous design approach for zero-liquid discharge evaporation systems. Journal of Cleaner Production, 140, 1399-1414, 2017.

[12] Janajreh, I., Zhang, H., El Kadi, K., & Ghaffour, N. Freeze Desalination: Current Research Development and Future Prospects. Water Research, 119389, 2022.

[13] Subramani, A., & Jacangelo, J. G. Emerging desalination technologies for water treatment: a critical review. Water research, 75, 164-187, 2015.

[14] Ahmed, F., Hashaikeh, R., and Hilal, N.. Hybrid technologies: The future of energy efficient desalination – a review. Desalination, 495:114659, 2020.

[15] Xie, C., Zhang, L., Liu, Y., Lv, Q., Ruan, G., and Hosseini, S.. A direct contact type ice generator for seawater freeze desalination using lng cold energy. Desalination, 435:293–300, 2018.

[16] Macias-Bu, L., Guerra-Valle, M., Petzold, G., Orellana-Palma, P.. Technical and environmental opportunities for freeze desalination. Separation & Purification Reviews, pages 1–10, 2022.

[17] Elhefny, A., Shabgard, H., Cai, J., Optimal freeze desalination configuration for maximum theoretical energy efficiency, 8th Thermal and Fluids Engineering Conference, MD, TFEC-2023-46410, 2023.

[18] Najim A. A review of advances in freeze desalination and future prospects. npj Clean Water, 19;5(1):1-5, 2022.
[19] Shafiur Rahman, M., Ahmed, M., Chen, X.. Freeze-melting process and desalination: I. review of the state-of-the-art. Separation & Purification Reviews, 35(02):59–96, 2006.
[20] Eghtesad, A., Salakhi, M., Afshin, H., & Hannani, S. K. Numerical investigation and optimization of indirect freeze desalination. Desalination, 481, 114378, 2020.
[21] Mistry, K., Lienhard, J.. Generalized least energy of separation for desalination and other chemical separation processes. Entropy, 15(6):2046–2080, 2013.
[22] Inc. OLI Systems. Add-in, aspen simulation workbook v12.1, 2022 from https://support.olisystems.com.
[23] Using oli in aspen plus user manual, 2022, from https://wiki.olisystems.com/wiki/using oli in aspen plus user manual.
[24] Water Condition & purification – Magazine, January 2005.
[25] Castillo-Téllez, B., Romero, R. J., Allaf, K., & Pilatowsky-Figueroa, I. Saline Diffusion Modeling for Sodium Chloride Aqueous Solutions: Freezing for Desalination Purposes. Separations, 9(10), 272, 2022.
[26] Song, J., Zhang, D., Yuan, H., Zhang, J., Zhou, P., Li, Y., & Mei, N. Sea water frozen crystalisation impacted by flow and heterogeneous nucleation: PFM-LBM coupled modeling, simulation and experiments. Desalination, 524, 115484, 2022.
[27] Chang, J., Zuo, J., Lu, K. J., & Chung, T. S. Freeze desalination of seawater using LNG cold energy. Water Research, 102, 282-293, 2016.
[28] Thijssen, H.A.C. Freeze concentration of food liquids, Proceedings SOS/70,
3rd International Congress of Food Science and Technology, Washington,DC; 491, 1970.
[29] Thijssen, H.A.C. Apparatus for separation and treatment of solid particles from a liquid suspension. U.S. Patent 3,872,009, 1975.
[30] Thijssen, H.A.C. Freeze concentration of food liquids. Food Manufacture, 44 (7): 49 – 54, 1969.
[31] Thijssen, H.A.C. Freeze concentration. In Advances in Preconcentration and Dehydration of Foods. Spicer, A. (ed.), John Wiley: New York, 115– 149, 1974.
[32] Thijssen, H.A.C. Current developments in the freeze concentration of liquid foods. In Freeze Drying and Advanced Food Technology, 1975.
[33] Shwartz, J. and Probstein, R.F. An analysis of counterwashers for freeze distillation desalination. Desalination, 4: 5 – 29, 1968.
[34] Mandri, Y., Rich, A., Mangin, D., Abderafi, S., Bebon, C., Semlali, N., Klein, J., Bounahmidi, T., & Bouhaouss, A. Parametric study of the sweating step in the seawater desalination process by indirect freezing. Desalination, 269(1-3), 142-147, 2011.
[35] Shone, R. D. C.. The freeze desalination of mine waters. Journal of the Southern African Institute of Mining and Metallurgy, 87(4), 107-112, 1987.

[36] Shabgard, H., Parthasarathy, R., Cai, J., Kaviani, R., Elhefny, A.. "Apparatus and method for continuous separation of solid particles from solid-liquid slurries." U.S. Patent Application 17/750,113, filed November 24, 2022.
[37] Attia, A. A. New proposed system for freeze water desalination using auto reversed R-22 vapor compression heat pump. Desalination, 254(1-3), 179-184, 2010.
[38] Bell, I., Wronski, J., Quoilin, S., Lemort, V.. Pure and pseudo-pure fluid thermophysical property evaluation and the open-source thermophysical property library coolprop. Industrial & Engineering Chemistry Research, 53(6):2498–2508, 2014.
[39] Wang, P., Anderko, A., & Young, R. D. A speciation-based model for mixed-solvent electrolyte systems. Fluid Phase Equilibria, 203(1-2), 141-176, 2002.
[40] Y. Marcus, Ion Properties, Marcel Dekker, New York, 1997.
[41] W. Linke, A. Seidell, Solubilities of Inorganic and Metal-Organic Compounds, Vols. 1 and 2, American Chemical Society, Washington, DC, 1965.
[42] H. Stephen, T. Stephen, Solubilities of Inorganic and Organic Compounds, Vols. 1 and 2, Pergamon Press, New York, 1979.
[43] H.L. Silcock, Solubilities of Inorganic and Organic Compounds, Vol. 3, Pergamon Press, New York, 1979.
[44] A. Maczynski, A. Skrzecz, TRC Data Bases for Chemical and Engineering. Floppy Books on VLE, LLE and SLE, 1995–1999.
[45] J. Gmehling, U. Onken, Vapor–Liquid Equilibrium Data Collection. Dechema Chemistry Data Series, 1977.
[46] S. Ohe, Vapor–Liquid Equilibrium Data—Salt Effect. Physical Sciences Data Series, No. 43, Elsevier, New York, 1991.
[47] J.J. Christensen, R.W. Hanks, R.M. Izatt, Handbook of Heats of Mixing, Wiley, New York, 1982.
[48] Y.P. Handa, G.C. Benson, Fluid Phase Equilib. 3 (1979) 185–249.
[49] O. Söhnel, P. Novotny, Densities of Aqueous Solutions of Inorganic Substances. Physical Sciences Data 22, Elsevier, New ` York, 1985
[50] P. Debye, E. Hückel, Phys. Z. 24 (1924) 185.
[51] R.A. Robinson, R.H. Stokes, Electrolyte Solutions, 2nd Edition, Butterworths, London, 1959.
[52] J.M. Prausnitz, R.N. Lichtenthaler, E.G. de Azevedo, Molecular Thermodynamics of Fluid-Phase Equilibria, 2nd Edition, Prentice-Hall, Englewood Cliffs, NJ, 1986.
[53] W.E. Acree Jr., Thermodynamic Properties of Nonelectrolyte Solutions, Academic Press, New York, 1984.
[54] Richardson, C. Phase relationships in sea ice as a function of temperature. Journal of Glaciology, 17(77), 507-519. 1976.
[55] Light, B., Brandt, R. E., & Warren, S. G.. Hydrohalite in cold sea ice: Laboratory observations of single crystals, surface accumulations, and migration rates under a temperature gradient, with application to “Snowball Earth”. Journal of Geophysical Research: Oceans, 114(C7), 2009.
[56] Lienhard, J., Mistry, K., Sharqawy, M., Thiel, G.. Thermodynamics, exergy, and energy efficiency in desalination systems. 2017.

[57] Mistry, K., McGovern, R., Thiel, G., Summers, E., Zubair, S., Lienhard, J.. Entropy generation analysis of desalination technologies. Entropy, 13(10):1829–1864, 2011.

Appendix A

Identifying the freeze desalination system's optimal configuration is the appendix's major focus. Multiple configurations have been investigated to help identify the most energy efficient freeze desalination system configuration. As described in Section 2, the optimal configuration is the one matching the benchmark values for the theoretical minimum work of separation for desalination [21] where the theoretical analysis adopted considers no irreversibility.

The first configuration investigated composes of a cascaded refrigeration cycle as presented in Fig. A1. The brine freezing chamber temperature equals the first stage evaporator temperature, the second stage condensing temperature equals the ambient temperature, and the evaporating temperature of the second stage equals the condensing temperature of the first stage. The inlet brine stream is logged to the brine freezing chamber to be cooled to the desired temperature. The cooled brine is then passed to a separator which perfectly separates the cold stream into pure ice and concentrate (highly concentrated un-frozen brine+ any formed solids).

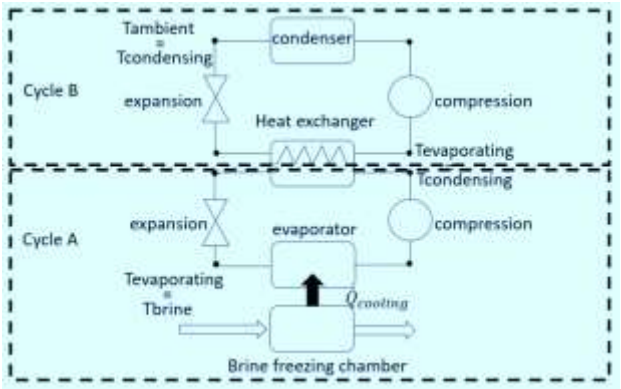

Fig. A1. FD system (configuration A) investigated as part of identifying the optimal configuration.

The second configuration analyzed is presented in Fig. A2. In this configuration, no mass of ice is being passed to the condenser's shell. Both separated cold streams are passed directly to parallel heat exchangers for precooling the inlet brine.

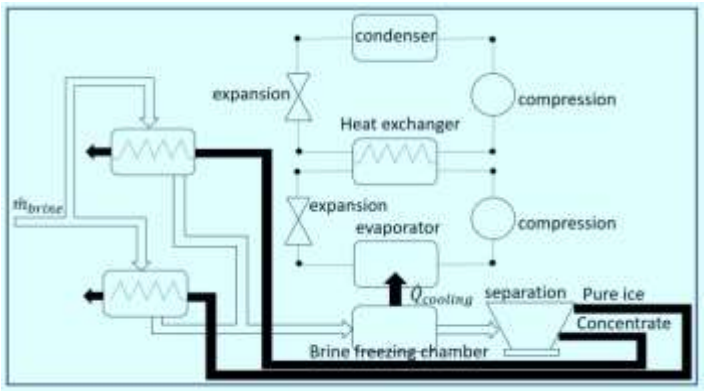

Fig. A2. FD system (configuration B) investigated as part of identifying the optimal configuration.

The temperature of the recovery streams exiting the brine precooling heat exchangers is rarely equal to the ambient temperature (25°C). This is because throughout the tested operational conditions, the ice doesn't melt completely as it precools the incoming brine stream. The detailed numerical proof is presented through Appendix C. Therefore, this configuration cannot be the optimal given that the recovery streams exit at temperatures lower than ambient failing to achieve maximum energy recovery.

Another configuration investigated is presented in Fig. A3 where both of the separated streams are directed to the condenser shell for energy recovery. The two streams exit the condenser's shell at 0 °C and are then passed to perform precooling of the brine entering the system.

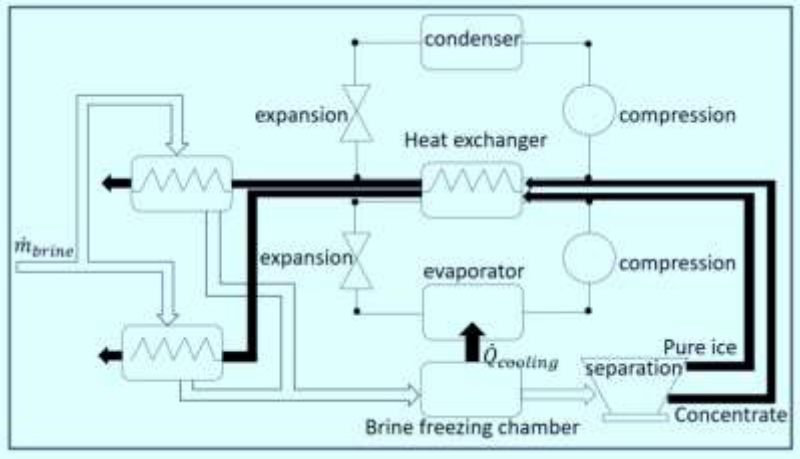

Fig. A3. FD system (configuration C) investigated as part of identifying the optimal configuration.

Figure A4 shows another FD configuration in which the cold concentrate stream is used to precool the inlet brine stream. The pure ice stream is first logged to the condenser shell for energy recovery while melting the ice. The stream exits the condenser shell as liquid H_2O at 0°C. The stream leaving the condenser shell is then passed to a precooler for cooling down the inlet brine.

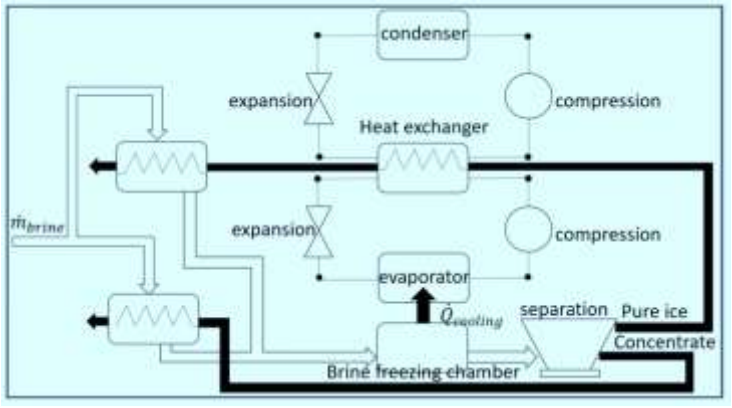

Fig. A4. FD system (configuration D) investigated as part of identifying the optimal configuration.

The cooling load and the work load considering Carnot refrigeration cycle were compared for all the investigated configurations. The FD system's configuration D (Fig. A4) showed the minimum energy consumption and matched the minimum work of separation for desalination [21] (validation presented in Section 6). Figure A5 shows the cooling load and work load associated with the optimum FD system configuration (D).

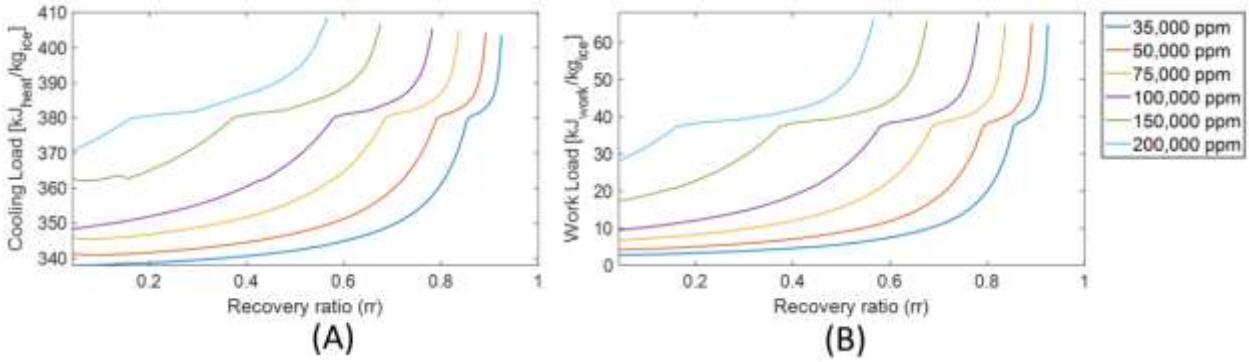

Fig. A5. Cooling load and work of separation at different recovery ratio values for refrigeration cycle configuration 4.

Appendix B

In this appendix, the correlation for finding the salinity of the treated water is deduced, based on mass balance of the salt through the desalination system (Eq. B.1).

$$m_{s,tw} + m_{s,rb} = m_{s,f} \quad \text{(B.1)}$$

The mass rate of salts can be replaced by the corresponding total mass rate (mass rate of salts + mass rate of water) multiplied by the salinity for each of the feed, treated and rejected streams. Thus, Eq. B.1 can be rewritten as Eq. B.2 and re-arranged in the form of Eq. B.3.

$$m_{tw}S_{tw} + m_{rb}S_{rb} = m_f S_f \quad \text{(B.2)}$$

$$\frac{m_{tw}}{m_f}S_{tw} + \frac{m_{rb}}{m_f}S_{rb} = S_f \quad \text{(B.3)}$$

The mass rate balance between the feed, treated and rejected streams (Eq. B.4) is applied to Eq. B.3 to obtain Eq. B.5.

$$m_{tw} + m_{rb} = m_f \quad \text{(B.4)}$$

$$\frac{m_{tw}}{m_f}S_{tw} + \frac{m_f - m_{tw}}{m_f}S_{rb} = S_f \quad \text{(B.5)}$$

The pure water recovery ratio (R) is defined as the ratio between the treated mass rate to the feed mass rate. Accordingly, Eq. B.5 can be rewritten as Eq. B.6 then re-arranged through Eq. B.7-B.9 to find the salinity of the rejected stream.

$$RS_{tw} + (1-R)S_{rb} = S_f \quad \text{(B.6)}$$

$$R\left(\frac{S_{tw}}{S_{rb}}\right) + (1-R) = \frac{S_f}{S_{rb}} \quad \text{(B.7)}$$

$$1 - R\left[1 - \left(\frac{S_{tw}}{S_{rb}}\right)\right] = \frac{S_f}{S_{rb}} \quad \text{(B.8)}$$

$$S_{rb} = \frac{S_f}{1 - R\left[1 - \left(\frac{S_{tw}}{S_{rb}}\right)\right]} \quad \text{(B.9)}$$

By multiplying the salinity of the rejected stream (presented by Eq. B.9) by the salinity ratio of the treated water to the rejected stream, the salinity of the treated water can be calculated using Eq. B.10.

$$S_{tw} = S_{rb}\left(\frac{S_{tw}}{S_{rb}}\right) = \left(\frac{S_{tw}}{S_{rb}}\right)\frac{S_f}{1 - R\left(1 - \frac{S_{tw}}{S_{rb}}\right)} \quad \text{(B.10)}$$

Appendix C

In the proposed optimal FD system configuration, the cascade coupling heat exchanger acts as a condenser for the refrigeration cycle 1 and an evaporator for the refrigeration cycle 2 (Fig. 1). In this study, we claim that the utilization of the cascade coupling heat exchanger as part of the optimal FD system configuration is essential to maximize the energy efficiency of the system. To support this claim, this section shows the steps for the investigation of the cooling energy recovery for the FD system without utilizing the cascade coupling heat exchanger. The outcomes prove and conclude this claim as explained in Section 3 of this paper.

The enthalpy method correlations are utilized to estimate the temperature and the ice fraction in the stream as presented in the following equations. The enthalpy is first estimated using Eq. (A.1), then the stream temperature is updated with Eq. (A.2). The crystalized ice fraction is estimated using Eq. (A.3) and the enthalpy of the stream at the current timestep is updated utilizing Eq. (A.4).

$$u\ \frac{\partial h}{\partial x} = UA\ (T_{st}\ - T_w) \tag{A.1}$$

$$T_{st} = \begin{cases} T_m + \dfrac{h}{C_s} & h \le 0 \\ T_m & 0 < h < h_{sl} \\ T_m + \dfrac{h\ - h_{sl}}{C_l} & h \ge h_{sl} \end{cases} \tag{A.2}$$

$$\phi_{ice} = \begin{cases} 1 & h \le 0 \\ 1 - \frac{h}{h_{sl}} & 0 < h < h_{sl} \\ 0 & h \ge h_{sl} \end{cases} \tag{A.3}$$

$$h_{st} = \begin{cases} C_s\ (T_{st} - \ T_m) & T_{st} < T_m \\ C_l\ (T_{st} - \ T_m)\ \ + \ h_{sl} & T_{st} > T_m \end{cases} \tag{A.4}$$

Fig. A1 shows an example of the thermal behavior of the return ice stream in the case of 35,000 ppm feed salinity, a freezing temperature of -35°C, ambient temperature of 25°C, and unfrozen brine stream (high salinity return liquid stream) resembling 2.5% of the mass of the return ice stream (unfrozen brine entrapped in pockets within the generated ice).

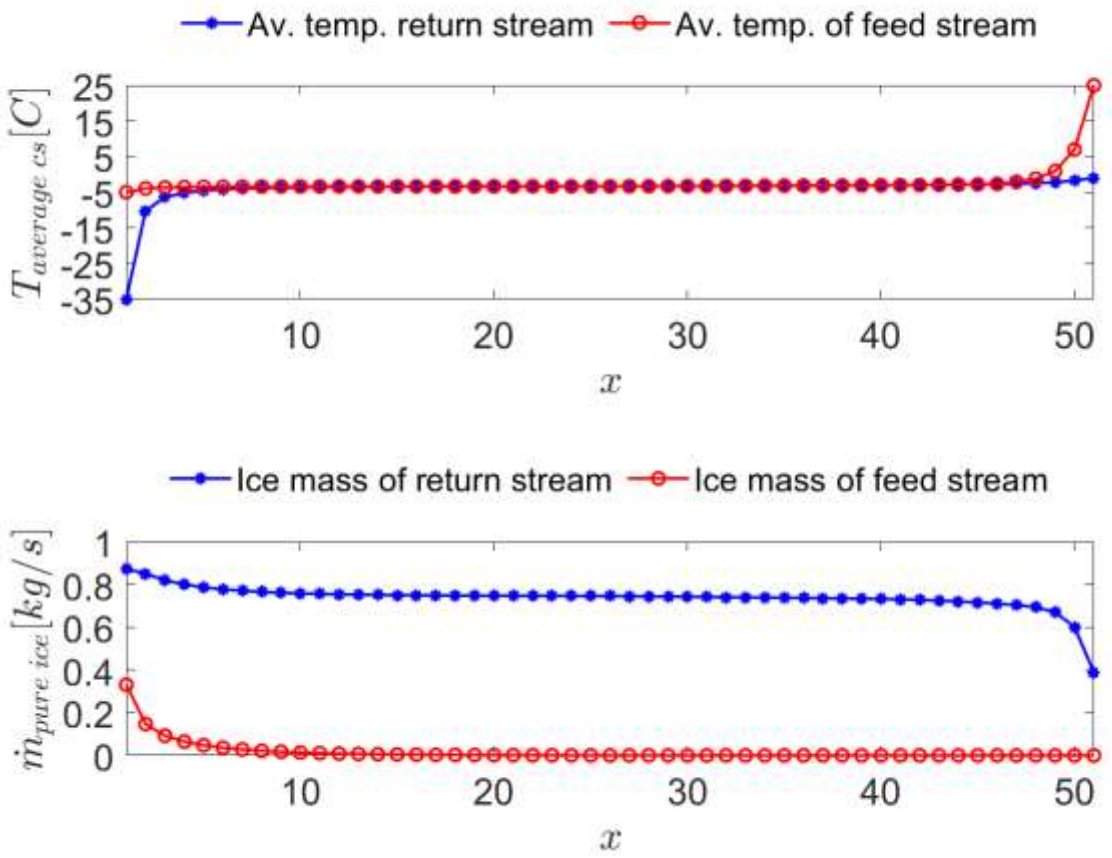

Fig. A1. Ice mass and temperature illustration along the FD system's precooler (without the cascade coupling heat exchanger).